2015

Structural evolution of electrodes in the NCR and CGR cathode-containing commercial lithium-ion batteries cycled between 3.0 and 4.5 V: an operando neutron powder-diffraction study

Wei Kong Pang
University of Wollongong, wkpang@uow.edu.au

Moshiul Alam
ANSTO

Vanessa K. Peterson
The Bragg Institute, Australian Nuclear Science And Technology Organisation, vep@ansto.gov.au

Neeraj Sharma
The Bragg Institute, University of New South Wales

Publication Details

Pang, W., Alam, M., Peterson, V. K. & Sharma, N. (2015). Structural evolution of electrodes in the NCR and CGR cathode-containing commercial lithium-ion batteries cycled between 3.0 and 4.5 V: an operando neutron powder-diffraction study. Journal of Materials Research, 30 (3), 373-380.

Structural evolution of electrodes in the NCR and CGR cathode-containing commercial lithium-ion batteries cycled between 3.0 and 4.5 V: an operando neutron powder-diffraction study

Abstract

The dissimilar lattice-evolution of the isostructural layered $Li(Ni,Co,Al)O_2$ (NCR) and $Li(Ni,Co,Mn)O_2$ (CGR) cathodes in commercial lithium-ion batteries during overcharging/discharging was examined using *operando* neutron powder-diffraction. The stacking axis (*c* parameter) of both cathodes expands on initial lithiation and contracts on further lithiation. Although both the initial increase and later decrease are smaller for the CGR cathode, the overall change between battery charged and discharged states of the c parameter is larger for the CGR (1.29%) than for the NCR cathode (0.33%). We find these differences are correlated to the transition metal to oxygen bond (as measured through the oxygen positional-parameter) which is specific to the different cathode chemistries. Finally, we note the formation of and suggest a model for a LiC_x intermediate between graphite and LiC_{12} in the anode of both batteries.

Keywords

operando, v, 5, 4, 3, between, cycled, batteries, ion, lithium, neutron, commercial, study, containing, cathode, cgr, ncr, electrodes, evolution, powder, diffraction, structural

Disciplines

Engineering | Science and Technology Studies

Publication Details

Pang, W., Alam, M., Peterson, V. K. & Sharma, N. (2015). Structural evolution of electrodes in the NCR and CGR cathode-containing commercial lithium-ion batteries cycled between 3.0 and 4.5 V: an operando neutron powder-diffraction study. Journal of Materials Research, 30 (3), 373-380.

Structural evolution of electrodes in the NCR and CGR cathode-containing commercial lithium-ion batteries cycled between 3.0 and 4.5 V: An *operando* neutron powder-diffraction study.

Wei Kong Pang[1,2,*], Moshiul Alam[1,3], Vanessa K. Peterson[1,*], Neeraj Sharma[3]

[1]*Australian Nuclear Science and Technology Organisation, Kirrawee DC NSW 2232, Australia*

[2]*School of Mechanical, Materials, and Mechatronic Engineering, Institute for Superconducting & Electronic Materials, Faculty of Engineering, University of Wollongong, NSW 2522, Australia*

[3]*School of Chemistry, UNSW Australia, Sydney NSW 2052, Australia*

**Corresponding authors.*

The dissimilar lattice-evolution of the iso-structural layered $Li(Ni,Co,Al)O_2$ (NCR) and $Li(Ni,Co,Mn)O_2$ (CGR) cathodes in commercial lithium-ion batteries during overcharging/discharging was examined using *operando* neutron powder-diffraction. The stacking axis (*c* parameter) of both cathodes expands on initial lithiation and contracts on further lithiation. Although both the initial increase and later decrease are smaller for the CGR cathode, the overall change between battery charged and discharged states of the *c* parameter is larger for the CGR (1.29%) than for the NCR cathode (0.33%). We find these differences are correlated to the transition metal to oxygen bond (as measured through the oxygen positional-parameter) which is specific to the different cathode chemistries. Finally, we note the formation and suggest a model for a LiC_x intermediate between graphite and LiC_{12} in the anode of both batteries.

Key words: Energy storage, neutron scattering, crystallographic structure.

1. INTRODUCTION

Lithium-ion batteries (LIBs) have higher energy densities, a portative design, and longer lifetimes than other battery technologies. Although LIBs meet the majority of the demands for existing smaller-scale applications (e.g. laptop computers and mobile phones), emerging larger-scale applications, such as electric vehicles and grid-scale energy storage, require improvements in safety, cost, energy density, and current performance.[1, 2] The first commercialized LIB by SONY Corp. in 1991 consisted of a layered $LiCoO_2$ cathode with a graphite anode.[3] Recently new cathode chemistries have been developed and commercialized both for specialist applications such as electric vehicles and to replace the more widespread use of $LiCoO_2$ cathodes. Such examples include $LiFePO_4$[4], $LiMn_2O_4$[5], and the mixed transition-metal $Li(Ni_{1/3}Mn_{1/3}Co_{1/3})O_2$ with varying Li:Ni:Co:Mn ratio, and Al-doped $Li(NiCo)O_2$,[6] with the latter two iso-structural to $LiCoO_2$[7]. The cathode plays an essential role in the performance of a LIB and is often the limiting factor in the battery's performance. The theoretical capacity of a cathode is limited by the composition, with $LiMO_2$ (M = transition metal) ~270–280 $mAh.g^{-1}$, $LiFePO_4$ ~170 $mAh.g^{-1}$, and $LiMn_2O_4$ ~148 $mAh.g^{-1}$. As the capacity of most cathodes is lower than that provided by the widely-used graphite anode (~ 372 $mAh.g^{-1}$), overcharging (over-delithiating) can seriously harm its structural stability and cycling performance, particularly for $LiMO_2$.[8]

The mixed transition-metal oxides generally have superior structural stability to $LiMO_2$, and for example, the mixed transition-metal $LiNi_{1/3}Co_{1/3}Mn_{1/3}O_2$ reported by Yabuuchi and Ohzuku is now commercially-used. Mn and Co are electrochemically inert in the active voltage range of $LiNi_{1/3}Co_{1/3}Mn_{1/3}O_2$, with the Ni valence changing from 2+ to 4+, effectively doubling the reversible capacity compared to $LiCoO_2$, from ~140 $mAh.g^{-1}$ to 200 $mAh.g^{-1}$.[7] By increasing the

Ni content, cathodes such as $LiNi_{0.8}Mn_{0.1}Co_{0.1}O_2$, $LiMn_{0.4}Ni_{0.4}Co_{0.2}O_2$, and Al-doped $Li(NiCo)O_2$[6, 9-12] deliver capacities higher than 200 $mAh.g^{-1}$.

Inert redox centers in the $R\bar{3}m$ mixed transition-metal structures make such materials more stable than $LiCoO_2$.[13] Reducing the Co content also reduces cost since the world Co price is currently determined by LIB demand, in addition to lowering the environmental impact, as Co is toxic. Although the as-prepared structure of such cathodes has been characterized, their structural evolution under different electrochemical conditions remains to be studied.

We have previously used *operando* neutron powder-diffraction (NPD) to show that the commercial NCR (of nominal composition $Li(Ni,Co,Al)O_2$) and CGR (of nominal composition $Li(Ni,Co,Mn)O_2$) cathodes have significantly different behaviors near the battery charged state.[14] Both cathodes expand along the stacking *c* axis during charge, while during the potentiostatic step recommended by the manufacturers, the CGR electrode stabilizes along the stacking *c* axis, whereas the NCR contracts significantly. On discharge, the NCR electrode expands for a short portion of discharge and subsequently contracts, while the CGR electrode only contracts. A related NPD study of the $Li(Ni_{0.5}Mn_{0.3}Co_{0.2})O_2$ cathode equilibrated at particular states of charge revealed a similar contraction near the battery charged state. This is thought to be related to cation mixing in the octahedral layers.[6] The differences in electrode evolution near the battery's charged state motivated this work, and we examine in detail the cathodes' structural evolution during discharge and charge following overcharge to 4.5 V (vs. the mesoporous microbead (MCMB) anode). The NCR cathode contains 3+ Co and Al, expected to be inert within the operating voltage of the battery and leading to the Ni being 3+ at full lithium occupancy and 4+ at the delithiated state. By comparison, the CGR cathode contains inert 4+ Mn and 3+ Co, leading to the Ni being 2+ at the fully lithiated state and 4+ at the delithiated state. Therefore,

these cathodes differ not only in their chemical composition but also in their redox transitions, which are Ni 3+/4+ and 2+/3+/4+ for the CGR and NCR cathodes, respectively.

As with our previous work,[14-16] we use non-destructive *operando* NPD to probe the cathode's structural evolution in commercial batteries. Earlier *in situ* NPD battery research involved data collected over extended periods of time for batteries equilibrated at a particular state-of-charge (SOC).[17, 18] More recent work has taken advantage of improved neutron sources and detectors to collect time-resolved *operando* NPD data, particularly for the $LiCoO_2$||graphite batteries, revealing the presence of new phases during charge/discharge,[13, 19] evaluating the nature of structural evolution,[12] and determining the influence of overcharging on the structure and electrochemical properties of electrodes.[20] NPD was used to study the changes in $LiCoO_2$ cathodes and carbon anodes with prolonged cycling and at two temperatures (25 and 50 °C).[21] Notably, only one previous study has used *in situ* NPD to understand the overcharging effects on commercial LIBs, revealing the structural changes in the graphite negative electrode. During overcharge, the graphite negative electrode converts to single-phase LiC_6, in contrast to conventional charge which results in the two-phase LiC_{12} and LiC_6 composition[22, 23] where the crystallographic structure of the LiC_{12} and LiC_6 phases were determined using NPD. Another lithiated phase intermediate between the graphite and LiC_{12} phase has been reported, and although this is thought to be of LiC_{24} or LiC_{18} composition,[22-29] the LiC_x composition and structure has not been fully established. Neutron radiography was used to elucidate lithium distribution under overcharging conditions in a coin cell with a carbon anode,[30] showing that lithium deposition is more likely to occur at the anode. Despite the detailed insights into overcharge phenomena revealed by neutron-based analysis,[15, 16] limited work has been carried out using *operando* NPD and is the focus here. We study the structural evolution of the CGR and

NCR cathodes, comparing their structural response during the first discharge and second charge following overcharge to 4.5 V (vs. MCMB). Additionally, we provide structural information concerning the LiC_x phase that is intermediate between graphite and LiC_{12}.

2. EXPERIMENTAL

18650-type LIBs were purchased with CGR and NCR cathodes, known as $Li(Ni,Co,Mn)O_2$ and $Li(Ni,Co,Al)O_2$, respectively. The CGR cathode composition is given as $LiNi_{1/3}Co_{1/3}Mn_{1/3}O_2$ in the information sheet provided by the manufacturer. The NCR cathode composition is given as a mixture of Ni, Co, and Al, although the Al is known to be a dopant with its concentration optimized for performance. These batteries are sold at a SOC ranging from 50-60%. Information regarding the battery composition, performance, and details are derived from the information sheet provided by the manufacturer. The batteries are rated to deliver 3.1 (NCR) and 2.25 (CGR) Ah using constant-current charging up to 4.2 V and holding using a tapering current (potentiostatic step). The exact weight of active cathode and anode material in these commercial batteries is unknown, although based on capacity ratings we expect at least 20 and 11 g of active cathode in the NCR and CGR batteries, respectively. *Operando* NPD data were collected on WOMBAT,[31] the high-intensity neutron powder diffractometer, at the Open Pool Australian Light-water (OPAL) reactor facility at the Australian Nuclear Science and Technology Organisation (ANSTO). The batteries were placed in a neutron beam of wavelength 2.4198(1) Å, determined using the NIST SRM 660b, and data were collected in the range $16.0° \leq 2\theta \leq 136°$. A schematic of the experiment setup is presented in Figure S1. NPD data were acquired every 3 min during charge/discharge cycling. NPD data correction, reduction, and visualization were undertaken using the program LAMP [32], with analyses carried out using both Rietveld and

single-peak fitting methods. The recommended voltage range for the batteries is 3.0-4.2 V, and during the NPD experiment the batteries were cycled galvanostatically between 3 and 4.5 V at a constant current of 0.5 A using an Autolab potentiostat/galvanostat (PG302N) under ambient conditions, with the external temperature maintained at 22.5 °C.

3. RESULTS AND DISCUSSION

The charge-discharge profiles of the batteries are shown in **Figure 1**, highlighting that the batteries were kept at 3.7-3.8 V during storage. We find that the NCR-containing battery delivers 99% of the rated discharge capacity whilst the CGR-containing battery exhibits 106.7% of the rated discharge capacity under overcharge conditions. This work compares the first discharge and second charge structural response of the NCR and CGR cathodes following the overcharge step and the electrochemical behavior of the corresponding battery. In the NCR cathode the 3+ Co and Al are inert within the operating voltage and the Ni valence is expected to be 3+ at full lithium occupancy. This may explain why the charge-discharge curve for the NCR-containing battery contains only 1 sloping plateau corresponding to the Ni^{3+}/Ni^{4+} couple, in comparison to the two features in the CGR-containing battery profile, corresponding to the $Ni^{2+}/Ni^{3+}/Ni^{4+}$ couples, where the CGR cathode contains 4+ Mn and 3+ Co and allows the Ni to be 2+.

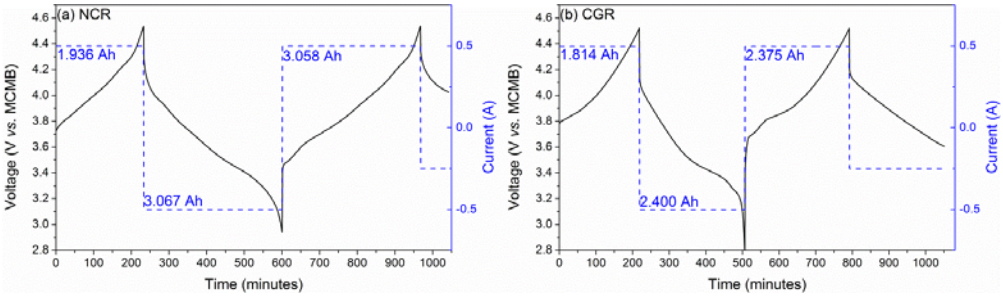

Figure 1. Charge-discharge profiles for (a) NCR and (b) CGR containing batteries obtained during *operando* NPD experiments.

The NPD patterns for both batteries are similar (**Figure S2**), as expected given their similar construction and components, with the notable exception of the intensity of reflections that is influenced by differences in the neutron scattering-length for the different transition metals. Given their dissimilar capacity, the cathodes are compared using their SOC (defined by the completeness of the anode transition). The cathode structures were refined using the data for the battery at the 100% SOC (voltage = 4.5 V *vs*. MCMB) (**Table SI**) and the parameters that were not expected to vary during battery cycling were fixed during the subsequent sequential refinement (e.g. those of Al and Cu current collectors). The evolution of the NCR and CGR 003 reflection is provided in support of the Rietveld-derived *c* lattice parameter. Similarly, the evolution of the NCR 101 and CGR 012 reflections support the Rietveld-derived *a* (= *b*) lattice parameter evolution, with the reflection choice guided by intensity differences and overlap with the anode reflections during cycling. **Figure 2** and **3** show results of single Gaussian peak-fitting of the NPD data alongside the sequentially-refined lattice parameters for the NCR and CGR cathodes. Rietveld-refinement profiles using the collected NPD data at the battery charged and discharged states are shown in Figure S3. The battery voltage curve and SOC is also given. The *c* lattice parameter of both cathodes increases and then decreases during discharge, with the reverse observed during charge. In contrast, the *a* lattice parameter for both cathodes increases monotonically during charge with the reverse occurring during discharge. The behaviour of the *c* lattice parameter of the CGR and NCR cathodes is relatively consistent with that of the iso-structural $LiCoO_2$ material.[8, 33, 34] The exception is the single-phase transition of the NCR and CGR cathodes compared with the small two-phase region of the $LiCoO_2$ material, composed of lithium-rich and lithium-poor phases,[35] exhibited throughout charge-discharge.

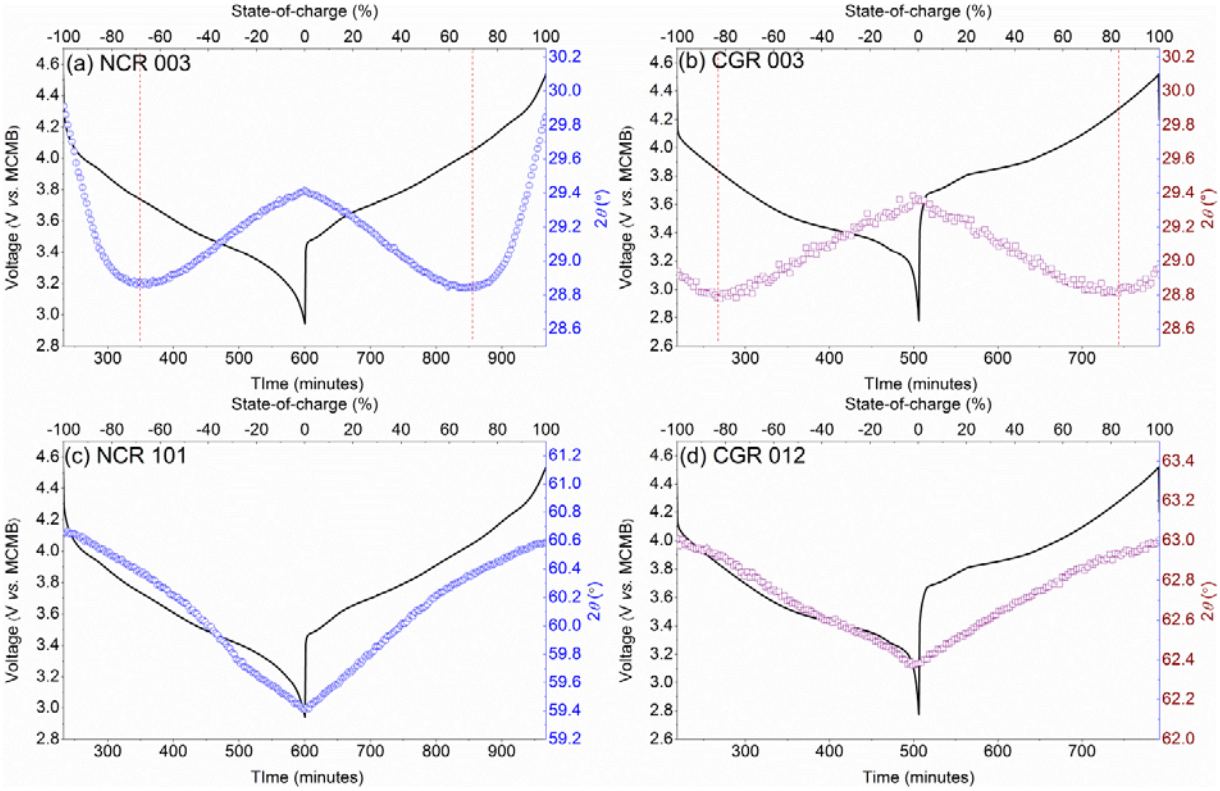

Figure 2. Results of single Gaussian peak-fitting of NCR and CGR cathode reflections. A negative SOC indicates discharge and a positive sign charge. Dotted lines denote the transition between increasing and decreasing *c* lattice parameter.

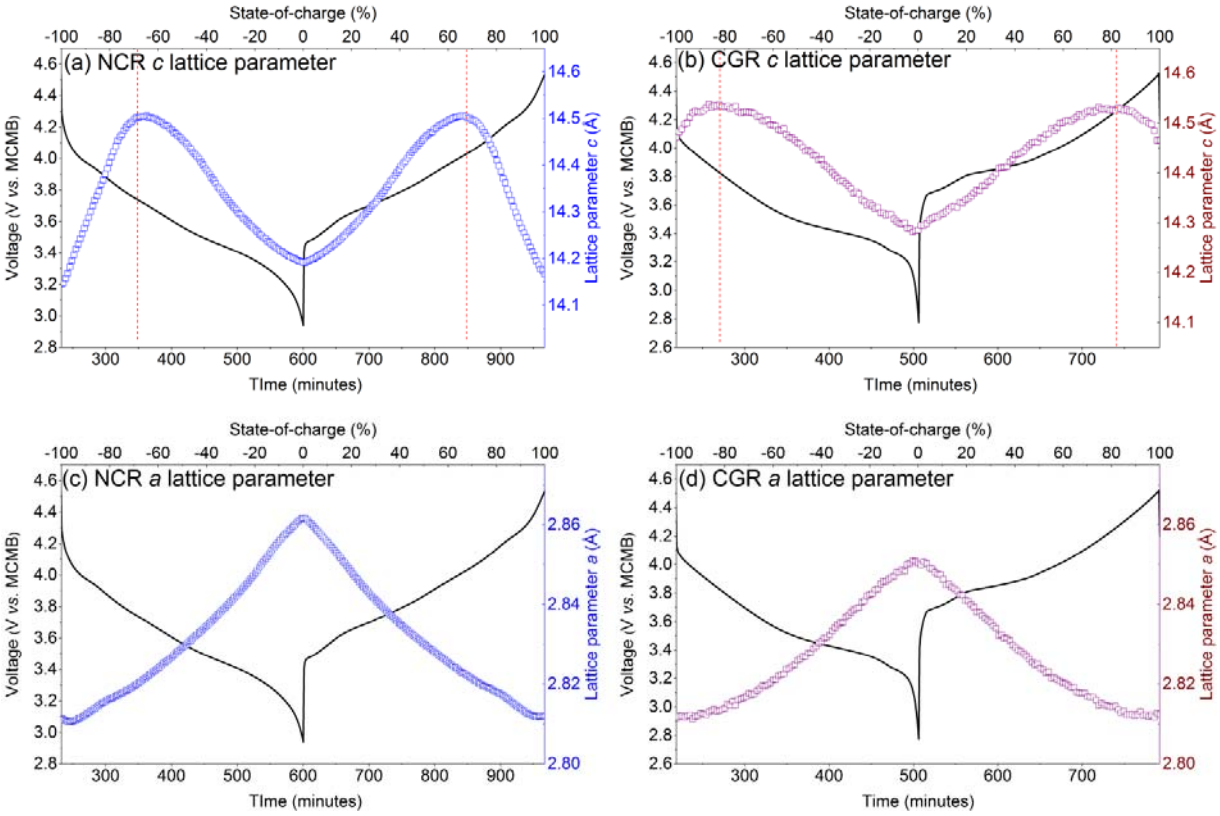

Figure 3. Refined lattice parameters for the NCR and CGR cathodes within batteries during discharge and charge. The dotted lines denote the inflexion point between the increase and decrease of the *c* lattice parameter.

At first the *c* lattice parameter for both CGR and NCR cathodes increases with Li content during discharge, obeying Vegard's law, with the subsequent non-Vegard decrease of the lattice parameter *c* ascribed to the electrostatic attraction between the O-containing layers as a result of the deficient average-charge of the O. The increase of the *a* lattice parameter during discharge arises from decreased attraction between lower oxidation-state transition metal (Ni) and O ions, expanding the transition-metal oxygen octahedra. The NCR and CGR cathode lattice at various battery SOC are summarised in **Table I**. Overall, the *c* lattice parameter in both cathodes changes less than the *a* lattice parameter during discharge and charge. Importantly, compared with the ~ 2.6% expansion of the *c* lattice parameter of $LiCoO_2$,[8, 33, 34] the *c* lattice parameter of

the NCR and CGR cathodes changes by only 0.33 and 1.29%, respectively, between SOC = 0 and 100%, suggesting possibly improved structural and cycling stability.

TABLE I. Lattice response of the NCR and CGR cathodes within a battery during cycling between 3.0 and 4.5 V at a constant current of 0.5 A.

Battery	Lattice parameter (Å)	SOC (%)*					Lattice parameter change (%)	
		-100	-68.96	0	67.26	100	Discharge[#]	Charge[^]
NCR	*c*	14.146(5)	14.502(5)	14.192(7)	14.505(6)	14.166(6)	0.33	-0.18
	a	2.8115(3)	2.8199(4)	2.8617(5)	2.8224(4)	2.8120(4)	1.79	-1.74

Battery	Lattice parameter (Å)	SOC (%)*					Lattice parameter change (%)	
		-100	-82.22	0	82.80	100	Discharge[#]	Charge[^]
CGR	*c*	14.472(7)	14.537(6)	14.286(5)	14.530(6)	14.466(7)	-1.29	1.26
	a	2.8115(7)	2.8133(5)	2.8503(5)	2.8136(7)	2.8124(7)	1.38	-1.33

*Negative and positive signs denote discharging and charging processes, respectively. [#]Change during 100-0% SOC. [^]Change during 0-100% SOC.

We note that the transition point between the Vegard and non-Vegard behaviour of the *c* lattice parameter occurred at a lower SOC (~ 68%) for the NCR-containing battery, relative to the CGR-containing battery (SOC ~ 82%). Also of note is that the lattice variation during cycling is larger than the variation between charged and discharged states, although the high reversibility of the lattice response is consistent with the excellent cycling stability of these cathodes.

Whilst the overall responses of the NCR and CGR cathode lattice is very similar, there is a notable difference in this behaviour near the fully charged and discharged states. We find that although the lattice parameter *c* of the CGR cathode is smallest at the discharged battery state, that for the NCR cathode is not, having a larger value at the discharged than charged state. To understand the larger contraction of the *c* lattice parameter of the CGR cathode relative to the NCR in the later stages of discharge, we examine the position of the O atom between the stacking axis layers. Rietveld refinement using the NPD data for the CGR and NCR-containing batteries allowed extraction of the oxygen position during lithium insertion and extraction (**Figure 4**). Clearly, the oxygen positional parameter of the CGR cathode changes significantly less than that of the NCR cathode, except for the near discharged state. During discharge, the oxygen positional parameter of the NCR cathode remained steady at approximately 0.253(1) before increasing to 0.262(1) at ~ 68% SOC and finally decreasing to 0.255(1) at 0% SOC. In contrast, the oxygen positional parameter of the CGR cathode varies subtly between 0.261(1) and 0.263(1), but drops significantly to 0.258(1) near the discharged state. The larger change in oxygen positional parameter during initial stages of discharge and final stages of charge are associated with the smallest *c* lattice parameter at ± 100% SOC in the NCR cathode, compared to a gradual change observed in the CGR cathode, where the *c* lattice parameter is smallest at the discharged state (0% SOC).

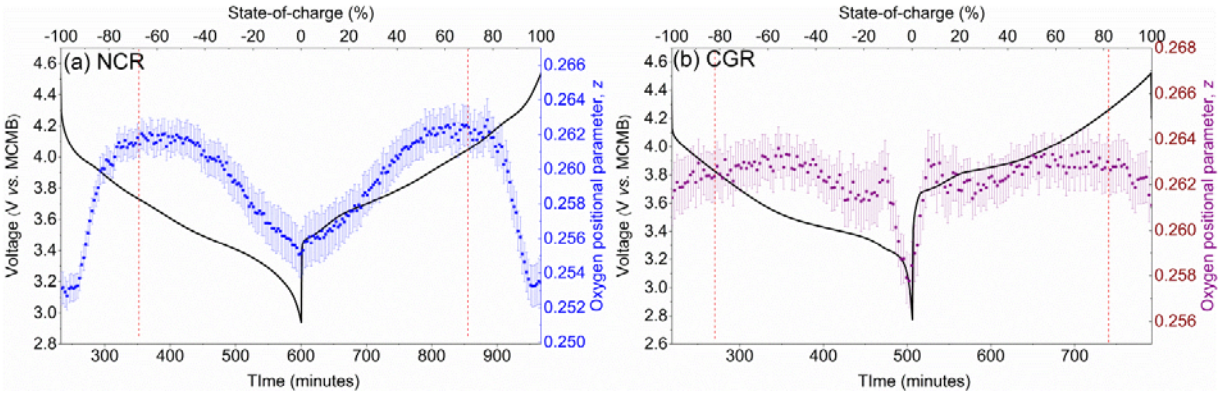

Figure 4. Variation of the oxygen positional parameter of the NCR (a) and CGR (b) cathodes within batteries during discharge and charge. Dotted lines denote the transition between increasing and decreasing *c* lattice parameter.

The graphitic anodes are identical in the two batteries and their evolution during cycling is expected to be similar. **Figure 5** shows a contour plot of the NPD data in the 2θ range 35-45°, detailing the evolution of the lithium-intercalated anode phases during battery charge and discharge. The positions of the reflections for these phases remain nearly unchanged during battery operation while the intensities vary, indicating that two-phase reactions occur. The NPD patterns for the as-obtained batteries in a wider 2θ range are shown in Figure S2. The stack plots in Figure 5 show clearly that multiple two-phase reactions of the anode occur, with the involved reflections associated with the formation of LiC_6, LiC_{12}, graphite, and an unknown LiC_x phase thought to have a lithium concentration intermediate between LiC_{12} and graphite. The LiC_x intermediate phase that occurs near discharged state before the formation of graphite has been previously noted although its stoichiometry is controversial.[22-29] Reflections from the LiC_x phase are observed at 40.71°, 75.45°, 88.57°, and 108.44°. Assuming that the LiC_x is a typical hexagonal structure, these reflections correspond to to *d*-spacings of 3.48 1.98, 1.74, and 1.49 Å with a 4.92 Å *a* lattice parameter and a 10.42 Å *c* lattice parameter. Based on the typical ~ 3.5 Å

spacing between graphene layers in lithiated graphitic anodes, this *c* lattice parameter suggests that the material contains 3 graphene layers that are ~ 3.47 Å apart. Assuming full occupation of lithium sites within the lithium-containing layers, the lattice parameter *a* suggests that *x* is 18. The four peaks that we see for the intermediate phase then correspond to the LiC_{18} 003, 202, 006, and the overlapping 205/007 reflections.

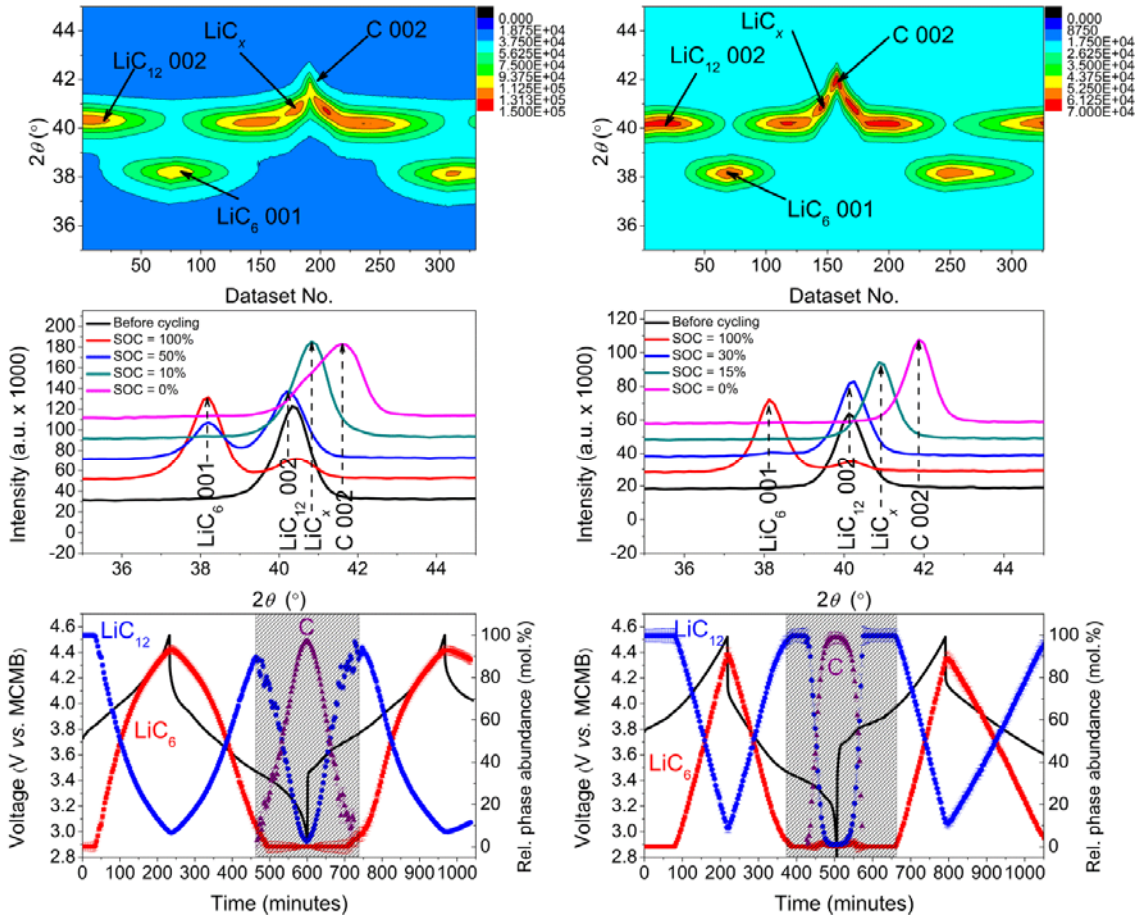

Figure 5. Data and results for the NCR-(left) and CGR-(right) containing batteries. Contour plot (upper) of NPD data within the 35-45° 2θ range (intensity scale is shown independently) and corresponding stack plot (middle) at various battery SOCs. The relative phase fractions of graphite, LiC_{12}, and LiC_6 (excluding the LiC_x phase in the shaded region) are also shown (bottom).

In both the NCR- and CGR-containing batteries the graphite phase appears near the fully-discharged state (0% SOC, 3.0 V). The data for the NCR-containing battery reveal there is ~ 93(2) mol.% LiC_6 and 7(1) mol.% LiC_{12} at 4.5 V, indicating that the LiC_{12}-LiC_6 two-phase reaction is incomplete even in the 4.5 V overcharged state. By definition, the SOC for NCR is approximately 93% of the theoretical value for graphite (the reaction of C to LiC_6). For the CGR-containing battery the NPD data indicate there is 91(4) mol.% LiC_6 and 9(3) mol.% LiC_{12} at the fully charged state (4.5 V). Similarly, the LiC_{12}-LiC_6 two-phase reaction is also incomplete in the CGR-containing battery, where the SOC is approximately 91% of the theoretical value for graphite.

4. CONCLUSIONS

Here we use *operando* neutron powder diffraction to measure the structural evolution of electrodes in commercial lithium-ion batteries during glavanostic cycling between 3.0 and 4.5 V and show the differences in these induced by different cathode chemistries. The NCR ($Li(Ni,Co,Al)O_2$) and CGR ($Li(Ni,Co,Mn)O_2$) cathodes adopt similar structures, and although they exhibit similar overall lattice evolution, there exist significant differences as a result of their composition. During lithiation on discharge, the *c* lattice parameter stacking axis first increases, obeying Vegard's law, and then decreases as a result of the deficient average-charge of the O ions and subsequent electrostatic attraction between the O-containing layers. The opposite occurs on delithiation during charge. Interestingly, the initial increase and later decrease is smaller (by ~ 82% and 19%, respectively,) for the CGR cathode than for the NCR cathode. The overall change of the NCR cathode between SOC = 0 and 100%, is 74% smaller than that of the CGR cathode, with the larger expansion of the CGR material corresponding to a larger variation of the oxygen

position between charged and discharged states. At the anode, during lithiation we find an intermediate LiC_x phase formed between LiC_{12} and graphite in both batteries that appears to be a LiC_{18} hexagonal structure with lattice parameters *c* and *a* of 10.42 and 4.94 Å, respectively.

ACKNOWLEDGEMENTS

The authors are also grateful to the staff members at the Bragg Institute, ANSTO for their operations support. Dr. Sharma would like to thank AINSE Ltd. for providing support through the research fellowship scheme.

References:

1. J.M. Tarascon and M. Armand: Issues and Challenges Facing Rechargeable Lithium Batteries *Nature.* **414**(6861), 359 (2001).
2. R. Berthelot, D. Carlier and C. Delmas: Electrochemical investigation of the P2–Na_xCoO_2 phase diagram *Nat. Mater.* **10**(1), 74 (2011).
3. Y. Nishi: Lithium ion secondary batteries; past 10 years and the future *J. Power Sources.* **100**(1–2), 101 (2001).
4. A.K. Padhi, K.S. Nanjundaswamy and J.B. Goodenough: Phospho olivines as Positive Electrode Materials for Rechargeable Lithium Batteries *J. Electrochem. Soc.* **144**(4), 1188 (1997).
5. M.M. Thackeray, A. de Kock, M.H. Rossouw, D. Liles, R. Bittihn and D. Hoge: Spinel electrodes from the Li-Mn-O system for rechargeable lithium battery applications *J. Electrochem. Soc.* **139**, 363 (1992).

6. O. Dolotko, A. Senyshyn, M.J. Mühlbauer, K. Nikolowski and H. Ehrenberg: Understanding structural changes in NMC Li-ion cells by in situ neutron diffraction *J. Power Sources.* **255**(0), 197 (2014).

7. N. Yabuuchi and T. Ohzuku: Novel lithium insertion material of $LiCo_{1/3}Ni_{1/3}Mn_{1/3}O_2$ for advanced lithium-ion batteries *J. Power Sources.* **119–121**(0), 171 (2003).

8. G.G. Amatucci, J.M. Tarascon and L.C. Klein: CoO_2, The End Member of the Li_xCoO_2 Solid Solution *J. Electrochem. Soc.* **143**(3), 1114 (1996).

9. S.J. Shi, Y.J. Mai, Y.Y. Tang, C.D. Gu, X.L. Wang and J.P. Tu: Preparation and electrochemical performance of ball-like $LiMn_{0.4}Ni_{0.4}Co_{0.2}O_2$ cathode materials *Electrochim. Acta.* **77**(0), 39 (2012).

10. H.-S. Kim, K.-T. Kim and P. Periasamy: Synthesis and Electrochemical Performances of $LiNi_{0.4}Mn_{0.4}Co_{0.2}O_2$ Cathode Material for Lithium Rechargeable Battery *Electronic Mater. Lett.* **2**(2), 119 (2006).

11. M.S. Idris and A.R. West: The Effect on Cathode Performance of Oxygen Non-Stoichiometry and Interlayer Mixing in Layered Rock Salt $LiNi_{0.8}Mn_{0.1}Co_{0.1}O_{2-\delta}$ *J. Electrochem. Soc.* **159**(4), A396 (2012).

12. G. Hu, W. Liu, Z. Peng, K. Du and Y. Cao: Synthesis and electrochemical properties of $LiNi_{0.8}Co_{0.15}Al_{0.05}O_2$ prepared from the precursor $Ni_{0.8}Co_{0.15}Al_{0.05}OOH$ *J. Power Sources.* **198**(0), 258 (2012).

13. S.C. Yin, Y.H. Rho, I. Swainson and L.F. Nazar: X-ray/Neutron Diffraction and Electrochemical Studies of Lithium De/Re-Intercalation in $Li_{1-x}Co_{1/3}Ni_{1/3}Mn_{1/3}O_2$ (x = 0 → 1) *Chem. Mater.* **18**(7), 1901 (2006).

14. M. Alam, T. Hanley, W.K. Pang, V.K. Peterson and N. Sharma: Comparison of the so-called CGR and NCR cathodes in commercial lithium-ion batteries using in situ neutron powder diffraction *Powder Diffr.* **In Press**, (2014).

15. W.K. Pang, V.K. Peterson, N. Sharma, J.-J. Shiu and S.-h. Wu: Lithium Migration in $Li_4Ti_5O_{12}$ Studied Using in Situ Neutron Powder Diffraction *Chem. Mater.* **26**(7), 2318 (2014).

16. W.K. Pang, N. Sharma, V.K. Peterson, J.-J. Shiu and S.-H. Wu: In-situ neutron diffraction study of the simultaneous structural evolution of a $LiNi_{0.5}Mn_{1.5}O_4$ cathode and a $Li_4Ti_5O_{12}$ anode in a $LiNi_{0.5}Mn_{1.5}O_4||Li_4Ti_5O_{12}$ full cell *J. Power Sources.* **246**(0), 464 (2014).

17. J. Shu: Study of the Interface Between $Li_4Ti_5O_{12}$ Electrodes and Standard Electrolyte Solutions in 0.0-5.0 V *Electrochem. Solid-State Lett.* **11**(12), A238 (2008).

18. V. Palomares, A. Goni, A. Iturrondobeitia, L. Lezama, I. de Meatza, M. Bengoechea and T. Rojo: Structural, magnetic and electrochemical study of a new active phase obtained by oxidation of a $LiFePO_4$/C composite *J. Mater. Chem.* **22**(11), 4735 (2012).

19. M. Armand and J.M. Tarascon: Building Better Batteries *Nature.* **451**, 652 (2008).

20. N. Sharma and V.K. Peterson: Overcharging a lithium-ion battery: Effect on the Li_xC_6 negative electrode determined by in situ neutron diffraction *J. Power Sources.* **244**(0), 695 (2013).

21. O. Dolotko, A. Senyshyn, M.J. Mühlbauer, K. Nikolowski, F. Scheiba and H. Ehrenberg: Fatigue Process in Li-Ion Cells: An In Situ Combined Neutron Diffraction and Electrochemical Study *J. Electrochem. Soc.* **159**(12), A2082 (2012).

22. D. Billaud, F.X. Henry, M. Lelaurain and P. Willmann: Revisited structures of dense and dilute stage II lithium-graphite intercalation compounds *J. Phys. Chem. Solids.* **57**(6–8), 775 (1996).

23. X.-L. Wang, K. An, L. Cai, Z. Feng, S.E. Nagler, C. Daniel, K.J. Rhodes, A.D. Stoica, H.D. Skorpenske, C. Liang, W. Zhang, J. Kim, Y. Qi and S.J. Harris: Visualizing the chemistry and structure dynamics in lithium-ion batteries by in-situ neutron diffraction *Sci. Rep.* **2**, (2012).

24. J.R. Dahn, R. Fong and M.J. Spoon: Suppression of staging in lithium-intercalated carbon by disorder in the host *Phys. Rev. B.* **42**(10), 6424 (1990).

25. D. Guerard and A. Herold: Intercalation of lithium into graphite and other carbons *Carbon.* **13**(4), 337 (1975).

26. P. Trucano and R. Chen: Structure of graphite by neutron diffraction *Nature.* **258**(5531), 136 (1975).

27. K.C. Woo, W.A. Kamitakahara, D.P. DiVincenzo, D.S. Robinson, H. Mertwoy, J.W. Milliken and J.E. Fischer: Effect of In-Plane Density on the Structural and Elastic Properties of Graphite Intercalation Compounds *Phys. Rev. Lett.* **50**(3), 182 (1983).

28. Y. Qi, H. Guo, L.G. Hector and A. Timmons: Threefold Increase in the Young's Modulus of Graphite Negative Electrode during Lithium Intercalation *J. Electrochem. Soc.* **157**(5), A558 (2010).

29. S.J. Harris, A. Timmons, D.R. Baker and C. Monroe: Direct in situ measurements of Li transport in Li-ion battery negative electrodes *Chem. Phys. Lett.* **485**(4–6), 265 (2010).

30. A. Same, V. Battaglia, H.-Y. Tang and J.W. Park: In situ neutron radiography analysis of graphite/NCA lithium-ion battery during overcharge *J. Appl. Electrochem.* **42**, 1 (2012).

31. A.J. Studer, M.E. Hagen and T.J. Noakes: Wombat: The high-intensity powder diffractometer at the OPAL reactor *Physica B*. **385–386, Part 2**(0), 1013 (2006).

32. D. Richard, M. Ferrand and G.J. Kearley: Large array manipulation program *J. Neutron Research.* **4**, 33 (1996).

33. A. Van der Ven, M.K. Aydinol, G. Ceder, G. Kresse and J. Hafner: First-principles investigation of phase stability in Li_xCoO_2 *Phys. Rev. B.* **58**(6), 2975 (1998).

34. S. Laubach, S. Laubach, P.C. Schmidt, D. Ensling, S. Schmid, W. Jaegermann, Thi, K. Nikolowski and H. Ehrenberg: Changes in the crystal and electronic structure of $LiCoO_2$ and $LiNiO_2$ upon Li intercalation and de-intercalation *Phys. Chem. Chem. Phys.* **11**(17), 3278 (2009).

35. N. Sharma, V.K. Peterson, M.M. Elcombe, M. Avdeev, A.J. Studer, N. Blagojevic, R. Yusoff and N. Kamarulzaman: Structural changes in a commercial lithium-ion battery during electrochemical cycling: An in situ neutron diffraction study *J. Power Sources.* **195**(24), 8258 (2010).

Supporting information

TABLE SI. Models of the NCR and CGR cathode (100% SOC) used in the sequential refinement.

NCR $Li(Ni_{0.6}Co_{0.3}Al_{0.1})O_2$ ($R\bar{3}m$)
Lattice parameters*
a = 2.8115(3) Å
c = 14.146 (5)Å

Atom	Site	x	y	z	U_{iso} (Å^2)	Occupancy
Li1	3*b*	0	0	½	0.2~	1~
Ni	3*a*	0	0	0	0.2~	0.6(1)^
Co	3*a*	0	0	0	0.2~	0.3(1)^
Al	3*a*	0	0	0	0.2~	0.1~
O1	6*c*	0	0	0.250(1)*	0.2~	1~

~ Fixed. ^ Value initially refined and then but fixed in the sequential refinement. *starting value, refined sequentially

CGR $Li(Ni_{1/3}Mn_{1/3}Co_{1/3})O_2$ ($R\bar{3}m$)
Lattice parameters*
a = 2.8115(7) Å
c = 14.472(7) Å

Atom	Site	x	y	z	U_{iso} (Å^2)	Occupancy
Li1	3*b*	0	0	½	0.2~	1~
Ni	3*a*	0	0	0	0.2~	1/3~
Mn	3*a*	0	0	0	0.2~	1/3~
Co	3*a*	0	0	0	0.2~	1/3~
O1	6*c*	0	0	0.2614(1)*	0.2~	1~

~ Fixed. *starting value, refined sequentially.

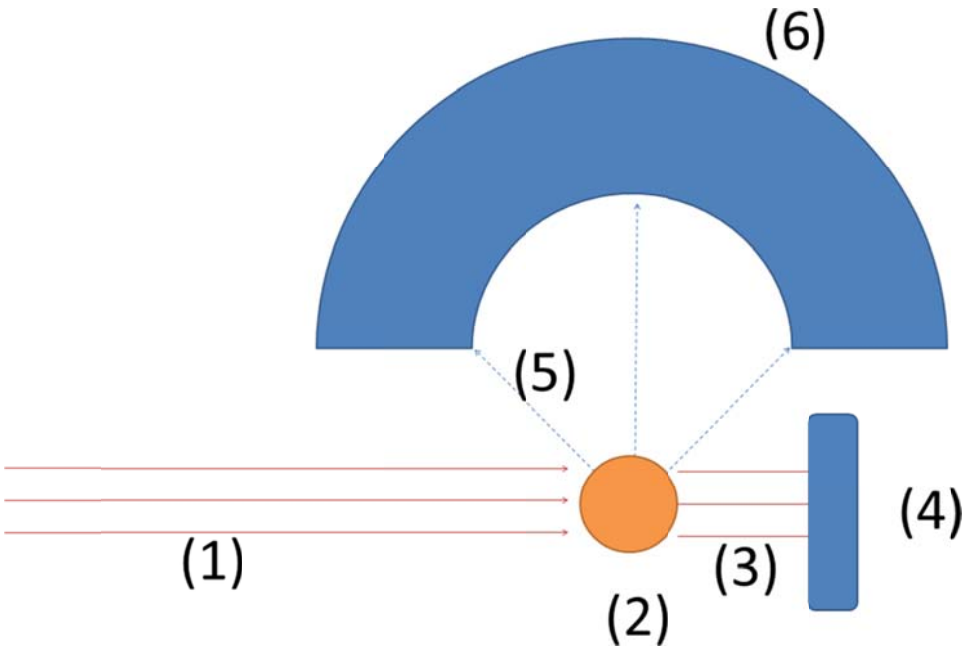

Figure S1. Schematic diagram illustrating the *operando* NPD experiment. (1) incident neutron beam, (2) battery on the sample stage, (3) transmitted neutron beam, (4) beam stop, (5) diffracted beams, and (6) 120-degree area detector.

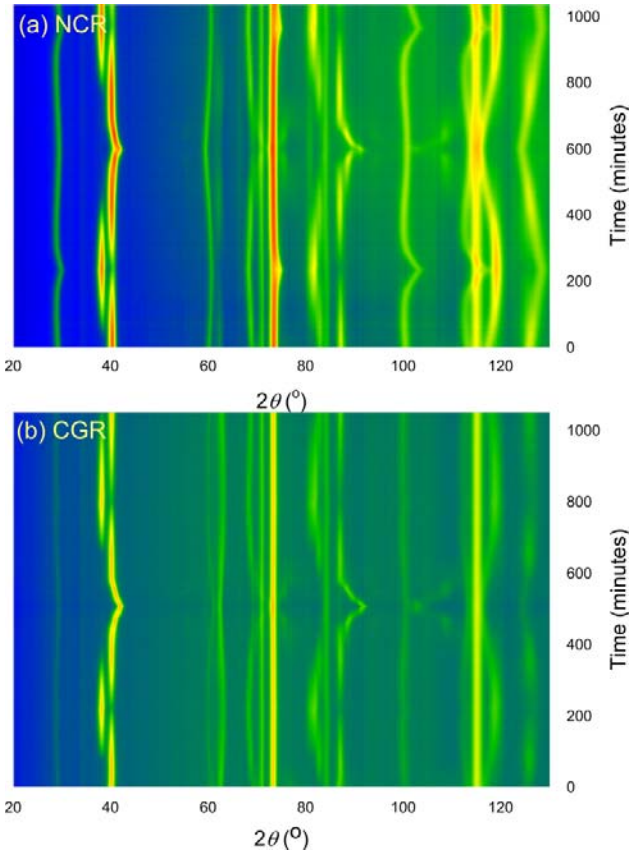

Figure S2. Contour plots of *operando* NPD data of (a) NCR- and (b) CGR-containing batteries.

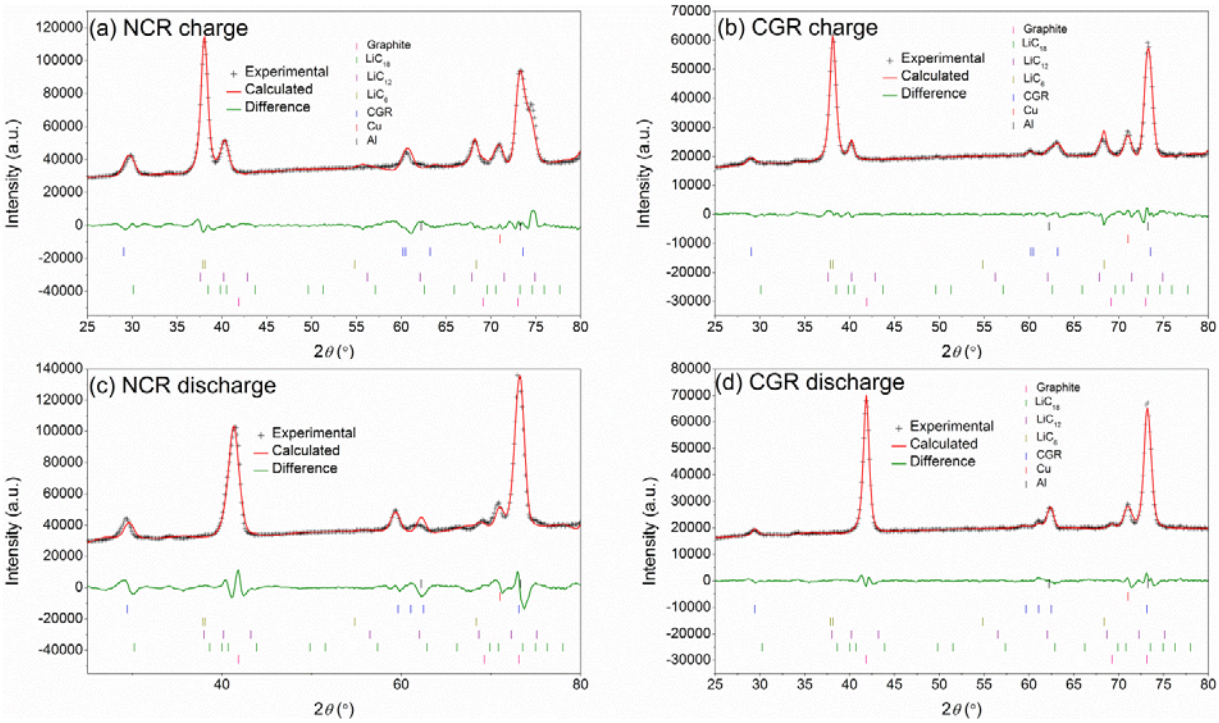

Figure S3. Refinement profiles for NPD data of NCR- and CGR-containing batteries at fully charged and discharged states. Range of refinement figures of merit for the entire dataset include the weighted profile R-factor (R_{wp}) = 15.2-26.6 for the NCR battery and R_{wp} = 12.2-18.8 for the CGR battery.